12. M. Greiner, C. A. Regal, J. T. Stewart, D. S. Jin, *Phys. Rev. Lett.* **94**, 110401 (2005).
13. M. Henny *et al.*, *Science* **284**, 296 (1999).
14. W. D. Oliver, J. Kim, R. C. Liu, Y. Yamamoto, *Science* **284**, 299 (1999).
15. H. Kiesel, A. Renz, F. Hasselbach, *Nature* **418**, 392 (2002).
16. Y. Kagan, B. V. Svistunov, G. V. Shlyapnikov, *Sov. Phys. JETP* **42**, 209 (1985).
17. E. A. Burt *et al.*, *Phys. Rev. Lett.* **79**, 337 (1997).
18. B. Laburthe Tolra *et al.*, *Phys. Rev. Lett.* **92**, 190401 (2004).
19. A. Robert *et al.*, *Science* **292**, 461 (2001); published online 22 March 2001 (10.1126/science.1060622).
20. O. Jagutzki *et al.*, *Nucl. Instrum. Methods Phys. Res. A* **477**, 244 (2004).
21. See supporting online materials on *Science* Online for details.
22. M. Naraschewski, R. Glauber, *Phys. Rev. A* **59**, 4595 (1999).
23. L. Deng *et al.*, *Nature* **398**, 218 (1999).
24. J. Vogels, K. Xu, W. Ketterle, *Phys. Rev. Lett.* **89**, 020401 (2002).
25. R. Stas, J. McNamara, W. Hogervorst, W. Vassen, *Phys. Rev. Lett.* **93**, 053001 (2004).
26. A. Öttl, S. Ritter, M. Köhl, T. Esslinger, *Phys. Rev. Lett.* **95**, 090404 (2005).
27. After submission of this manuscript, we became aware of a related experiment concerning atom correlations in an atom laser (*26*). We thank R. Sellem of the Détection Temps, Position Image Technology Division (supported by the Mission Ressources et Compétences Technologiques–CNRS Federation FR2764 and by the Université Paris-Sud) for a decisive role in the development of the time-to-digital converter, and O. Jagutzki for advice on delay lines.

Supporting Online Material
www.sciencemag.org/cgi/content/full/1118024/DC1
SOM Text

27 July 2005; accepted 5 September 2005
Published online 15 September 2005;
10.1126/science.1118024
Include this information when citing this paper.

Quantum Coherence in an Optical Modulator

S. G. Carter,[1]* V. Birkedal,[1]† C. S. Wang,[2] L. A. Coldren,[2] A. V. Maslov,[3] D. S. Citrin,[4,5] M. S. Sherwin[1]‡

Semiconductor quantum well electroabsorption modulators are widely used to modulate near-infrared (NIR) radiation at frequencies below 0.1 terahertz (THz). Here, the NIR absorption of undoped quantum wells was modulated by strong electric fields with frequencies between 1.5 and 3.9 THz. The THz field coupled two excited states (excitons) of the quantum wells, as manifested by a new THz frequency- and power-dependent NIR absorption line. Nonperturbative theory and experiment indicate that the THz field generated a coherent quantum superposition of an absorbing and a nonabsorbing exciton. This quantum coherence may yield new applications for quantum well modulators in optical communications.

Quantum three-state systems in which two of the states are strongly coupled by an intense laser field have been widely studied in atomic and molecular systems (*1*). The energies of the quantum states are altered as they are "dressed" by the strong light-matter interaction. Such dressed states were first observed by Autler and Townes (AT) in a molecular system driven by a strong radio-frequency field and probed by weak microwaves (*2*). When a radio-frequency resonance occurred, the microwave absorption line split in two. In three-state systems with weak coupling to the environment, AT splitting can evolve into electromagnetically induced transparency (EIT), in which a strong coupling beam induces transparency at a resonance at which the undriven system is opaque (*3*). This transparency is due to quantum interference between the dressed states. EIT is the basis for slow (*4*) and stopped light (*5*, *6*) in atomic systems.

A variety of quantum systems similar to atomic three-state systems can be engineered in semiconductor quantum wells (QWs). A QW is a layer of one semiconductor grown between semiconductors with larger band gaps (*7*). The layer with the smaller gap is sufficiently thin that well-defined sets of quantized states, or subbands, are associated with electron motion parallel to the growth direction. Within each subband, there is a continuum of states associated with different momenta parallel to the plane of the QW (perpendicular to the growth direction). AT-like splitting (*8*), quantum interference (*9*, *10*), and EIT (*11*, *12*) have been reported in QWs, but their observation has been more difficult than in atoms and molecules. This is in part because of much larger absorption linewidths, which result from disorder, from stronger coupling to the environment, or from scattering between subbands.

We have fabricated a particularly simple three-level system in undoped QWs (Fig. 1). The excitation with the lowest frequency occurs at about 350 THz (wavelength 857 nm or energy 1.46 eV) when an electron is promoted from the filled valence subband of highest energy (labeled h1) to the empty conduction subband of lowest energy (labeled e1). The excited electron binds with the hole it left behind to form an exciton with a hydrogen-like wave function in the QW plane. Transitions between different in-plane states (e.g., the 1s and 2p states) are allowed only for in-plane THz polarizations (*13*, *14*), which are not present in the experiments discussed here. The lowest exciton state is labeled h1X. The next exciton state, h2X, consists of an electron from e1 and a hole from the second highest valence subband, h2. NIR transitions between the crystal ground state and h2X are not allowed because of quantum mechanical selection rules. However, intersubband transitions from h1X to h2X are allowed for THz radiation polarized in the growth direction. The three states analogous to those in an AT picture are the crystal ground state, the lowest exciton h1X, and the second exciton h2X (*15*).

This report explores the NIR absorption of undoped QWs at low temperatures (~10 K) when they are driven by strong electric fields polarized in the growth direction with frequencies between 1.5 and 3.9 THz. Because the frequency of the THz laser is about 1% of that required to create an exciton, the strong laser field does not alter the populations of the quantum states of the system. Near 3.4 THz, the drive frequency is resonant with the transition between the two lowest exciton states. The AT splitting of excitons driven by strong intersubband radiation is experimentally observed, and theoretical predictions (*16*, *17*) are confirmed.

The sample consists of 10 $In_{0.06}Ga_{0.94}As$ QWs (each 143 Å) separated by $Al_{0.3}Ga_{0.7}As$ barriers (300 Å). InGaAs QWs were used instead of GaAs QWs so that the GaAs substrate was transparent for NIR light near the exciton energies. A 100-nm layer of aluminum was deposited on the surface of the sample on which the QWs were grown. The metallic boundary condition improved THz coupling and ensured that the THz field at the QWs was polarized almost perfectly in the growth direction (*18*). The interband absorption was probed using broadband, incoherent, NIR light from an 850-nm light-emitting diode focused onto the sample backside to a spot size ~250 μm in diameter. The NIR intensity was less than 0.3 W/cm^2. As illustrated in Fig. 1, the NIR beam was transmitted through the transparent substrate, interacted with the QWs, was reflected off of the Al layer, and was then collected and sent to a monochromator with an intensified charge-coupled device detector. The reflected NIR beam was measured during the 1 to 1.5 μs at the peak of the THz

[1]Physics Department and Institute for Quantum and Complex Dynamics (iQCD), Broida Hall Building 572, Room 3410, [2]Electrical and Computer Engineering Department, University of California, Santa Barbara, CA 93106, USA. [3]Center for Nanotechnology, NASA Ames Research Center, MS 229-1, Moffett Field, CA 94035, USA. [4]Electrical and Computer Engineering, Georgia Institute of Technology, Atlanta, GA 30332, USA. [5]Georgia Tech Lorraine, Metz Technopole, 2-3 rue Marconi, 57070 Metz, France.

*Present address: JILA, University of Colorado, 440 UCB, Boulder, CO 80309, USA.
†née Ciulin. Present address: Department of Chemistry, University of Aarhus, Langelandsgade 140, DK-8000 Århus C, Denmark.
‡To whom correspondence should be addressed. E-mail: sherwin@physics.ucsb.edu

pulse (fig. S2). The sample was mounted in a closed-cycle refrigerator and maintained at a temperature near 10 K. The lowest curves in Fig. 1, A to C, display the NIR reflectivity measured without the THz field. (The reflectivity is essentially double-pass transmission in this geometry.) The strong absorption line is from h1X. As expected, no absorption is observed from h2X. The energy of h2X is expected to be ~3.34 THz (13.8 meV) above h1X from calculations (*19*).

The THz radiation, given by the UCSB Free-Electron Lasers, was focused onto the edge of the sample with an off-axis parabolic mirror. The spot size was ~400 μm in diameter for THz frequencies between 2.5 and 3.9 THz, near the h1X-h2X resonance. The THz beam was on for ~4 μs with a repetition rate near 1 Hz. The maximum peak power incident on the sample was ~2 kW, giving a maximum intensity in the sample of ~1 MW/cm^2 (~15 kV/cm electric field amplitude). [This estimate of the electric field ignores propagation inside the sample and the Al coating on the surface (*18*)].

The effect of the THz field on the sample reflectivity was quite striking (Fig. 1, A to C). Each graph displays the reflectivity for a series of THz intensities. In Fig. 1A the THz frequency is f_{THz} = 2.52 THz, below the expected h1X-h2X resonance. As the THz intensity increased, the absorption line redshifted and a weaker absorption line appeared above the undriven exciton energy. Near the expected resonance, at f_{THz} = 3.42 THz (Fig. 1B), there was a clear symmetric splitting of the exciton line, which increased as a function of intensity. Just above the resonance, at f_{THz} = 3.90 THz (Fig. 1C), a weaker absorption line appeared below the undriven exciton energy. These measurements were carried out at ~10 K, but the splitting at f_{THz} = 3.42 THz was observed at temperatures up to 78 K.

The calculated reflectivity of a THz-driven QW is shown in Fig. 2 for THz intensities that give spectra comparable to those in Fig. 1. These results were obtained by numerically solving the Schrödinger equation for the dynamics of an optically created electron-hole pair in an infinitely deep QW. The quantization of the electron-hole states, the Coulomb interaction, and the THz field are all treated on an equal footing, without resorting to perturbation theory [see (*20*) for more details]. In essence, the THz field rocks the QW potential, which couples the various confined QW states in a dynamic fashion. All of the QW states are included in the calculations. This approach is equivalent to solving the polarization equation of the semiconductor Bloch equations (SBEs) in the low-density limit (*21*). The reflectivity is defined as the fraction of the incident optical power at a given NIR frequency that is not absorbed.

For these calculations, the absorption strength and energy position of h1X for zero

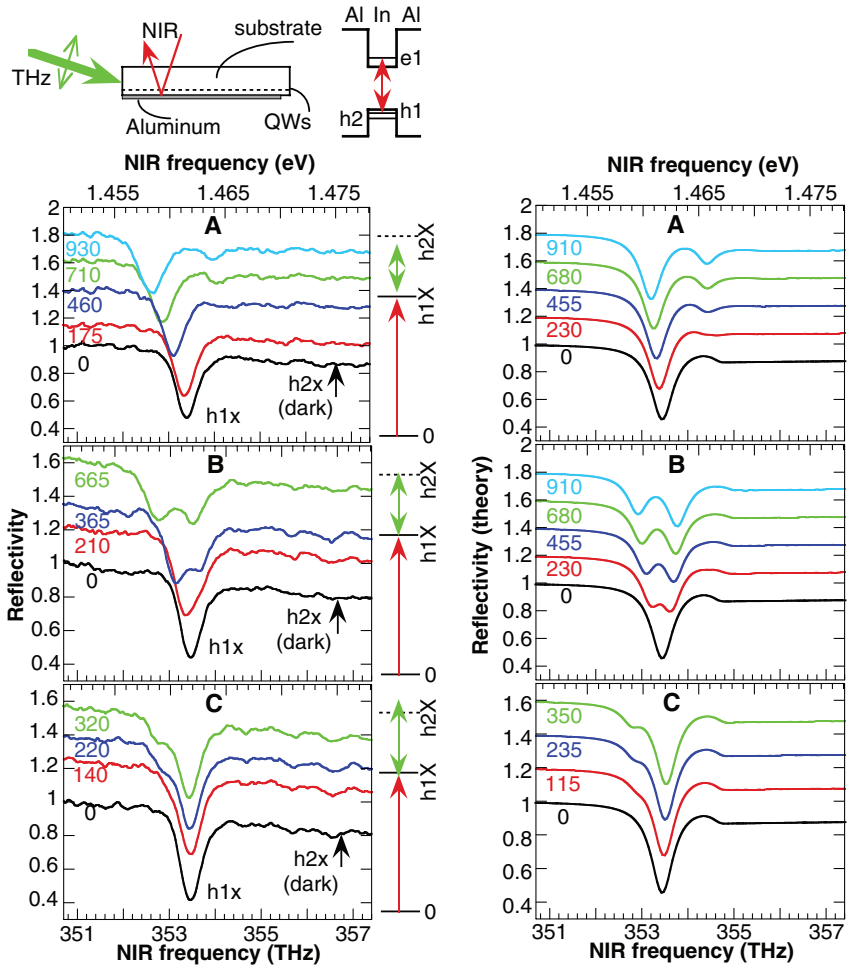

Fig. 1 (left). Reflectivity spectra for a series of THz intensities at f_{THz} = (**A**) 2.52 THz, (**B**) 3.42 THz, and (**C**) 3.90 THz. The spectra are offset and labeled according to the THz intensities (in kW/cm^2). Level diagrams illustrating the detuning from the expected h1X-h2X resonance are shown to the right of each graph. A schematic of the experimental geometry and the band diagram of a QW along with the relevant subband energies are displayed above. The red arrow represents the lowest excitation of the system, the h1X exciton. The AlGaAs barriers are labeled "Al" and the InGaAs layer is labeled "In." **Fig. 2 (right).** Calculated reflectivity spectra for a series of THz intensities at f_{THz} = (**A**) 2.52 THz, (**B**) 3.42 THz, and (**C**) 3.90 THz. The spectra are offset and labeled according to the THz intensity (in kW/cm^2). The absorption strength and energy position of the spectrum for zero THz field were set to best fit the measured reflectivity.

THz field were set to best fit the measured reflectivity. The calculated reflectivity in the presence of the THz field is qualitatively similar to the measured reflectivity, although small differences can be seen. It appears that the calculated splitting at 3.42 THz is more asymmetric than that observed experimentally, indicating that the experimental h1X-h2X resonance is closer to 3.42 THz than 3.34 THz. Also, there is an overall redshift of the measured reflectivity with increasing THz intensity that does not appear in the calculated spectra. This redshift is most likely due to heating by the THz beam and can clearly be seen in fig. S1A, where the absorption line positions are plotted as a function of intensity. The separation between the two absorption lines on resonance at f_{THz} = 3.42 THz is plotted as a function of intensity in fig. S1B. The splitting is discernible over a factor of ~4 in THz intensity (~2 in THz field). Theory and experiment are not far from one another over this limited range, although the dependence of the splitting on THz intensity is closer to a line than the square root function predicted by theory. More work must be done to characterize and understand the dependence of the splitting on THz intensity (*18*).

The reflectivity was measured at many THz frequencies from f_{THz} = 1.53 to 3.90 THz. Absorption spectra for f_{THz} = 2.82 through 3.90 THz (Fig. 3) were obtained by subtracting a linear decrease in reflectivity over the measured NIR frequency span and then calculating the negative natural logarithm of the reflectivity. These absorption spectra were then fit to two Lorentzians. The spectra at f_{THz} = 1.53, 1.98, and 2.52 THz (not shown) were more difficult to fit because the second absorption line was so weak. Differential spectra (spec-

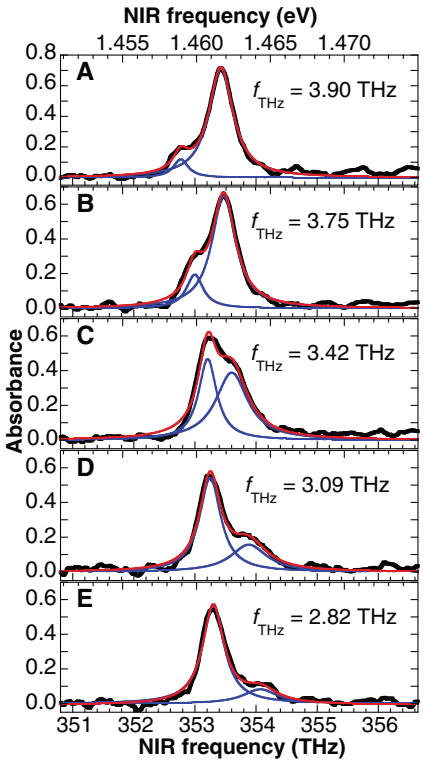

Fig. 3. Absorption spectra and fits for f_{THz} = 3.90 THz (**A**) to 2.82 THz (**E**). The black lines represent the absorption obtained from the reflectivity spectra by correcting for the downward slope due to continuum absorption and by taking the negative natural logarithm. The red curves are fits to two Lorentzians; the blue curves are the individual Lorentzians.

trum with THz field minus spectrum without THz field divided by spectrum without THz field) were used to determine the absorption line positions.

Figure 4 displays the absorption line positions as a function of THz frequency. The spectra used were all obtained with a THz intensity near 300 kW/cm^2 (within 10%), relatively low because this was the highest available intensity at f_{THz} = 3.75 THz and 3.90 THz. The anticrossing behavior in Fig. 4 near the h1X-h2X resonance is expected for the AT effect. The two absorption lines are associated with the two excitons dressed by the THz field. On resonance, the oscillator strength is shared equally between the two dressed states and the two absorption peaks are equal in magnitude. Off-resonance, the oscillator strength is strongest for the absorption line nearest the undriven exciton line. For low THz frequencies, the weaker peak approaches the h2X energy. The data points connected by solid lines in Fig. 4 are the results of calculations using the model equivalent to the SBE for an intensity of 375 kW/cm^2, which agree well with the measurements. The disagreement at 1.53 and 1.98 THz (lower positions) may be due to uncertainty in the THz intensity (*18*).

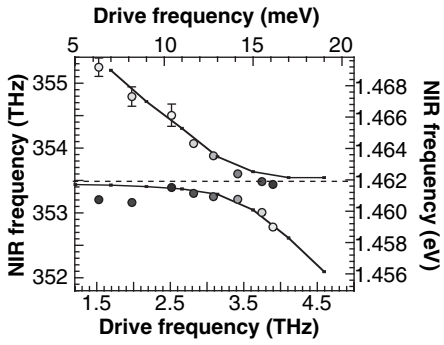

Fig. 4. Measured absorption line positions (large circles) versus THz frequency for a THz intensity of ~300 kW/cm^2. The absorption strength for each point is represented on a grayscale; darker circles indicate stronger absorption. The standard error of the positions from fitting is indicated by error bars except where smaller than the circle diameter. The data points and solid line represent the calculated absorption positions at a THz intensity of 375 kW/cm^2. Near the resonance at f_{THz} = 3.4 THz, the calculated spectra were fit to two Lorentzians to determine absorption positions; away from resonance, the positions were taken at the minimum of the reflectivity for each peak. The horizontal dashed line marks the undriven exciton line position.

Quantum wells driven by growth-direction electric fields are already important as electroabsorption modulators for fiber-optic communications operating with bandwidths <100 GHz (0.1 THz) (*22*). The basis for the QW modulators (QWMs) is the dc quantum-confined Stark effect, wherein a dc electric field polarized in the growth direction causes a redshift of the h1x absorption (*23*). The operating frequencies of QWMs are smaller than the exciton's linewidth. Thus, the response is adiabatic: The NIR absorption spectrum at any instant is determined only by the electric field at that same instant, and not by the modulation frequency. Modulation at higher frequencies is desirable given the 50-THz bandwidth of optical fibers.

Our results show that fascinating quantum effects occur when QWMs are driven in the high-frequency diabatic limit. Most important, AT splitting of excitons due to a strong THz field has been observed. The decrease in absorption at the undriven exciton resonance in the presence of the THz field is certainly suggestive of EIT, although the linewidth of h2X is not expected to be narrow enough for the required quantum interference effects.

The observation of dressed states in this system is noteworthy for several reasons. First, the effects have been observed over a wide range of THz frequencies, where the detuning from the resonance was comparable to the drive frequency. Observation of dressed states at large detunings is possible because the Rabi frequency (half the splitting on resonance) is relatively large, up to 20% of the drive frequency on resonance. Second, the THz driving field does not generate any excited-state population, in part because it is at a much lower frequency than the probe. The driving field is also quasi–continuous wave, which is rare for observations of coherent strong-field effects in semiconductors. Finally, applications to optical communications have been proposed for the THz-driven QW. Two NIR lasers resonant with different dressed states of this system interact strongly (*24*), leading to mutual transparency of the beams depending on their relative phases. This effect could be used for intermodulation of laser beams at arbitrarily low NIR intensities.

References and Notes

1. M. O. Scully, M. S. Zubairy, *Quantum Optics* (Cambridge Univ. Press, New York, 1997), chap. 7.
2. S. H. Autler, C. H. Townes, *Phys. Rev.* **100**, 703 (1955).
3. S. E. Harris, *Phys. Today* **50**, 36 (July 1997).
4. L. V. Hau, S. E. Harris, Z. Dutton, C. H. Behroozi, *Nature* **397**, 594 (1999).
5. C. Liu, Z. Dutton, C. H. Behroozi, L. V. Hau, *Nature* **409**, 490 (2001).
6. D. F. Phillips, A. Fleischhauer, A. Mair, R. L. Walsworth, M. D. Lukin, *Phys. Rev. Lett.* **86**, 783 (2001).
7. J. H. Davies, *The Physics of Low-Dimensional Semiconductors, an Introduction* (Cambridge Univ. Press, New York, 1998).
8. J. F. Dynes, M. D. Frogley, M. Beck, J. Faist, C. C. Phillips, *Phys. Rev. Lett.* **94**, 157403 (2005).
9. J. Faist *et al.*, *Opt. Lett.* **21**, 985 (1996).
10. H. Schmidt, K. L. Campman, A. C. Gossard, A. Imamoglu, *Appl. Phys. Lett.* **70**, 3455 (1997).
11. G. B. Serapiglia, E. Paspalakis, C. Sirtori, K. L. Vodopyanov, C. C. Phillips, *Phys. Rev. Lett.* **84**, 1019 (2000).
12. M. C. Phillips *et al.*, *Phys. Rev. Lett.* **91**, 183602 (2003).
13. K. B. Nordstrom *et al.*, *Phys. Rev. Lett.* **81**, 457 (1998).
14. S. Hughes, D. S. Citrin, *Phys. Rev. B* **59**, R5288 (1999).
15. The exciton states discussed are those with a 1s in-plane wave function, as these dominate the NIR spectra. The subbands h1 and h2 are "heavy hole" subbands because of their high effective masses. Excitons formed from the valence subbands with a lighter effective mass ("light hole" subbands) are shifted to higher energies as a result of strain and do not appear in the measured spectra. Excitons associated with higher subbands (e2, h3) are sufficiently far away in energy that they should only weakly couple to h1X.
16. A. Liu, C. Z. Ning, *J. Opt. Soc. Am. B* **17**, 433 (2000).
17. A. V. Maslov, D. S. Citrin, *Phys. Rev. B* **62**, 16686 (2000).
18. See supporting data on *Science* Online.
19. All calculations were performed for a 150 Å QW with infinite barriers. The electron and hole effective masses (for the growth direction) were 0.067 m_0 and 0.36 m_0, respectively.
20. A. V. Maslov, D. S. Citrin, *IEEE J. Sel. Top. Quantum Electron.* **8**, 457 (2002).
21. H. Haug, S. W. Koch, *Quantum Theory of the Optical and Electronic Properties of Semiconductors* (World Scientific, River Edge, NJ, ed. 4, 2004).
22. D. A. B. Miller, *Opt. Photon. News* **1**, 7 (1990).
23. S. Schmitt-Rink, D. Chemla, D. A. B. Miller, *Adv. Phys.* **38**, 89 (1989).
24. A. V. Maslov, D. S. Citrin, *J. Opt. Soc. Am. B* **19**, 1905 (2002).

25. Supported by NSF grants DMR 0244390 (S.G.C., V.B., M.S.S.) and DMR 0305524 (D.S.C.) and by Sun Microsystems. We thank D. Allen, R. Owings, D. Bouwmeester, and A. Wodtke for helpful feedback on the manuscript, and D. Enyeart for skillful operation of the UCSB Free-Electron Lasers.

Supporting Online Material

www.sciencemag.org/cgi/content/full/310/5748/651/DC1
SOM Text
Figs. S1 and S2

16 June 2005; accepted 21 September 2005
10.1126/science.1116195